Breaking AB stacking order in graphite oxide: *ab initio* approach

Dinh Loc Duong,[a] Gunn Kim,[ab] Hae-Kyung Jeong[a] and Young Hee Lee*[a]

Different bulk structures of graphite oxide were systematically investigated using density functional theory (DFT). Our model consisted of a hexagonal in-plane structure of graphene with hydroxyl and epoxide groups, and different oxidation levels and water content. The graphitic AB stacking order was stable in anhydrous graphite oxide, independent of oxidation levels. The hydrogen bonding interaction of layers became weaker as the oxidation level increased to the saturation limit. When water molecules were present in highly oxidized graphite oxide, the AB stacking order was broken due to entropic disorder. The interlayer distances increased with the oxidation level: the interlayer distance was 5.1 Å for low oxidation graphite oxide and 5.8 Å for high oxidation graphite oxide. The calculated interlayer distance of hydrated graphite oxide was 7.3 Å, which is in excellent agreement with experimental observations.

1. Introduction

Graphite oxide is used in thin film technologies because of its hexagonal in-plane structure and ability to be exfoliated layer by layer. Large-scale graphene can be produced by overlapping patches of dispersed graphite oxide layers followed by chemical reduction.[1,2] Graphite oxide can also be used as a precursor to form polystyrene–graphene composites and transparent conducting film.[3,4] Furthermore, graphite oxide can be used for the electrodes of batteries and supercapacitors because of its large interlayer distance.[5,6]

Graphite oxide with different oxidation levels can be synthesized by several methods.[7–13] Several models have been proposed to describe the structure of different graphite oxide species, and were summarized in a review article by Szabó. In general, graphite oxide has a layered structure with oxygen atoms and hydroxyl (–OH) groups distributed on buckled hexagonal carbon layers. The carboxyl and alkyl groups are located at the edge of graphite oxide flake.[12] The interlayer distance varies from 5.6 to 10 Å and this distance is dependent on the oxidation level and the amount of intercalated water.[9–12] However, the arrangement of oxygen atoms and hydroxyl groups is still unclear.

Several groups have confirmed experimentally that epoxide (1, 2 ether) groups formed by the oxygen atoms are randomly located in the graphene layer, and that epoxide and hydroxyl groups are adjacent to each other.[9,12,14] However, it is still unclear how one graphite oxide layer interacts with the adjacent layers, as this has never been clarified experimentally. Some theoretical studies of the structures and mechanical properties of oxidized graphene (single layer graphite oxide) have been performed.[15–19] Paci *et al.* have used randomly positioned epoxide and hydroxyl groups in the supercell of a large number of atoms to describe defects and estimated the interlayer distance of saturated graphite oxide. The interlayer distance of this saturated graphite oxide structure was 5.8 Å.[17] The interlayer distance has also been calculated theoretically using an AB stacking model by Boukhvalov and Katsnelson.[18] However, this model considered the interlayer distance of graphite oxide only with –OH groups; water was not taken into account. The estimated interlayer distance of this anhydrous graphite oxide model was 7 Å. This value, however, is not applicable to the actual structure of graphite oxide, because it is extremely difficult to obtain graphite oxide without intercalated water molecules. Furthermore, the AB stacking order of graphite oxide was not carefully considered in this model.

In the present work, we concentrate on the graphite oxide structure with the AB stacking order. The purpose of this paper is threefold: (i) to design a structural model of graphite oxide with different oxidation levels and intercalated water molecules, (ii) to determine the fully optimized interlayer distance, and (iii) to elucidate the breaking criteria of the AB stacking order and the underlying mechanism. To address these aims, we constructed three-dimensional structural models of graphite oxide with various oxidation levels and water contents based on density functional calculations using the generalized gradient approximation (GGA). The relative positions of epoxide and hydroxyl groups were optimized. The obtained interlayer distances are in excellent agreement with experimental values. Furthermore, the AB stacking order of anhydrous graphite oxide was preserved, regardless of the oxidation level. However, the AB stacking order was broken in hydrated graphite oxide with high levels of oxidation; it is attributed to the increase in the entropic disorder caused by the presence of water molecules.

2. Computational methods

Density functional calculations were carried out to optimize various graphite oxide structures. Wave functions were

[a] Department of Physics, Department of Energy Science, Sungkyunkwan Advanced Institute of Nanotechnology, Center for Nanotubes and Nanostructured Composites, Sungkyunkwan University, Suwon 440-746, South Korea.
E-mail: leeyoung@skku.edu; Fax: +82-31-290-5954
[b] Frontier Physics Research Division, Department of Physics and Astronomy, Seoul National University, Seoul 151-747, South Korea

expanded with a plane wave basis set implemented in the PWscf package.[20] Ultrasoft pseudopotentials were employed with the generalized gradient approximation for exchange and correlation in the Perdew–Burke–Ernzerhof functional.[21–23] The Brillouin zone was sampled with a $4 \times 4 \times 1$ irreducible Monkhorst–Pack k-point grid.[24] The kinetic energy cut-off for wave functions was 35 Ry (475 eV) for all atoms and the convergence threshold for calculation of self-consistent energy was 10^{-6} Ry ($\sim 10^{-5}$ eV). Our model structures were relaxed until the forces on the atoms were smaller than 0.025 eV Å^{-1}.

Graphite oxide species with low and high levels of oxidation were considered. The chemical formulae of low and high oxidation graphite oxide species are $C_8O(OH)$ and $C_8O_2(OH)_2$, respectively. The former species corresponds to that observed experimentally based on stoichiometry, while the latter species corresponds to graphite oxide with saturated oxygen and hydrogen content. Atomic forces and the total energy of a single layer graphene with epoxide and hydroxyl groups were minimized similar to the previous work.[19] The lowest energy configuration was then used to construct the bulk structure of graphite oxide. The unit cell used to form a bulk graphite oxide structure had two graphitic AB stacking layers of sixteen carbon atoms. For higher oxidation limit, we tried two hydroxyl groups that are located in the opposite side of the graphene layer. This turned out to give rise to higher energy. Therefore, we restricted our geometry to have functional groups in the same side of the graphene layer. The average distance between AB stacking layers was 6 Å initially. The unit cell was then optimized using the Broyden–Fletcher–Goldfarb–Shanno method (for stress minimization). For each oxidation level, symmetric (S) and asymmetric (A) positions of the epoxide and hydroxyl groups in the A layer with respect to the B layer were chosen, as shown in Fig. 1. The positions of functional groups are indicated by a series of numbers (primed) in the A (B) layer. Several orientations and relative shifts of the A layer with respect to the B layer were optimized to obtain the minimum energy configurations. Similar approaches were taken in the presence of water molecules. In this case, several positions of water molecules were considered for geometry optimization. Two water molecules were introduced in the unit cell; this corresponds to a wt% increase of 14 and 11% for less oxidized and highly oxidized graphite oxide, respectively.

To check the reliability of the calculational method, water dimer was optimized using our GGA–PBE method. The errors of interaction energy, O–O and O···H bond distance compared to experimental data[25] were −0.016 eV, −0.07 Å, and 0.02 Å, respectively. These values were also consistent with other calculations[25–28] and they are summarized in Table 1. To check the validity of the cell size, the cell size was doubled to ($8 \times 8 \times 1$). No appreciable geometry changes were observed with the doubled supercell. The relative energy value was changed but the order of the relative stability between given structures was not altered.

3. Results and discussion

3.1 Low oxidation graphite oxide, $C_8O(OH)$

The original unit cell was assumed to be hexagonal. Fig. 2 shows three different configurations obtained from optimizations. The lowest energy configuration, denoted by A(78-5′7′) and shown in Fig. 2(a), was used as the reference. The AB stacking order was well preserved. The corresponding parameters are listed in Table 2. The cell parameters match a hexagonal phase with some distortions in angles (α and β) from the c-axis. The interlayer distance is 5.1 Å. This value is smaller than the interlayer distances observed (6–8 Å).[9–11] This is most likely because actual samples usually contain water molecules.[7–11] Models that consider intercalated water molecules will be discussed later in this section. Some other locally stable configurations with slightly higher energy than that of the

Fig. 1 The difference of unit cells used to construct the $C_8O(OH)$ structure.
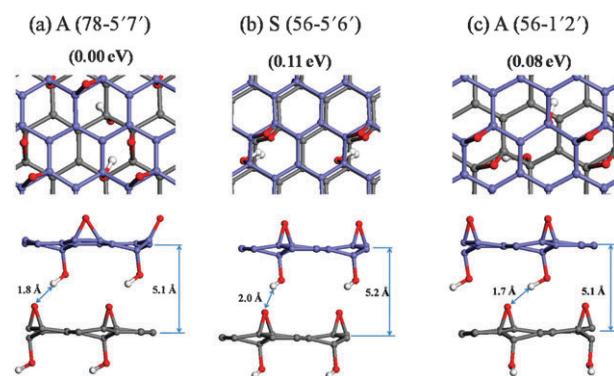
Fig. 2 Optimized configurations of $C_8O(OH)$ along the c vector direction (top panel) and side view (bottom panel) of the different relative arrangements of the epoxide and hydroxyl groups on the AB layers.

Table 2 Optimized (initial) configuration of the $C_8O(OH)$ structure

Model		A(78-5'7')	S(56-5'6')	A(56-1'2')
Cell parameters	a/Å	4.972 (5.1)	4.997 (5.1)	4.968 (5.1)
	b/Å	4.971 (5.1)	4.979 (5.1)	4.976 (5.1)
	c/Å	10.232 (12)	10.518 (12)	10.210 (12)
	α/°	91.8 (90)	83.7 (90)	80.8 (90)
	β/°	90.8 (90)	99.2 (90)	93.3 (90)
	γ/°	119.7 (120)	120.3 (120)	119.7 (120)
OH···O (epoxide) bonding angle/°		164	147	161
Relative energy/eV		0	0.11	0.08

reference configuration were found, as shown in Fig. 2(b and c). While the interlayer distances were similar to that of the reference, the AB stacking was transformed into the AA stacking in the case of S(56-5'6') and severely distorted in the case of A(56-1'2').

It is interesting to evaluate how the interlayer distance is maintained. The distance between an O atom in an epoxide group and an H atom in a hydroxyl group of the A(78-5'7') model was 1.8 Å, which is slightly shorter than the 2.0 Å of the S(56-5'6') model. Although this difference may be correlated to the electrostatic energy, and thus may explain the difference in the binding energy, this argument fails to explain the energetics of the A(56-1'2') model. We found that the net charge in the OH group and an adjacent carbon atom was nearly zero; this indicates that the dipole interaction may play an important role. This was confirmed by the bond angle between the hydroxyl group of the A layer and the oxygen of the epoxide group in the B layer, as shown in Table 2. We

conclude that hydrogen bonding stabilizes large interlayer distances in low oxidation graphite oxide structures.

3.2 High oxidation graphite oxide, $C_8O_2(OH)_2$

We next considered another graphite oxide configuration with high oxygen content.[10] Fig. 3 shows three locally stable configurations. The AB stacking order was still preserved in A(12-45-1'2'-5'7'). The interlayer distance was expanded to 5.8 Å. This value is consistent with the randomly positioned epoxide and hydroxyl group of the supercell with a large number of atoms.[17] As seen at the bottom of Fig. 3(a), the distance between H in the OH group and O in the same layer was 1.9 Å, which is shorter than the interlayer hydrogen bonding distances (2.5 and 2.6 Å, respectively). Therefore, the hydrogen bonding in the same layer is not negligible. Some other stable configurations with higher energies are also shown in Fig. 3(b and c). The AB stacking order was distorted in both cases, as shown in the top panels. This distortion is also evident from the deviations (α and β) from 90° in Table 3. Similar to the graphite oxide with low oxidation, the bond angles between OH and O in different models followed the energetics listed in Table 3.

The total electron charge distributions at the middle of the layer are shown in Fig. 4. We chose the most stable configurations of low and high oxidation states. Unlike graphite, which shows nearly uniform charge distribution in the middle of the layer, the charge densities were partially localized near the functional groups in graphite oxide. In the case of low oxidation graphite oxide, electron charges were
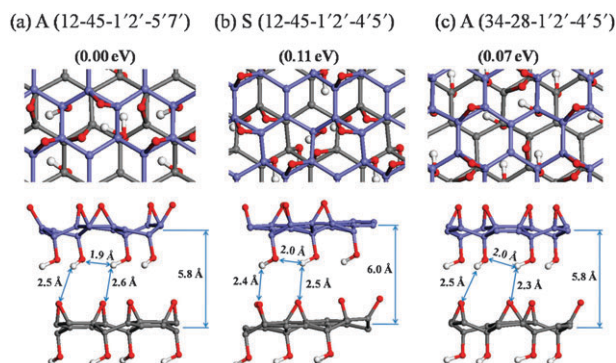
Fig. 3 Optimized configurations of $C_8O_2(OH)_2$ along the c vector direction (top panel) and side view (bottom panel) of the different relative arrangements of the epoxide and hydroxyl groups on the AB layers.
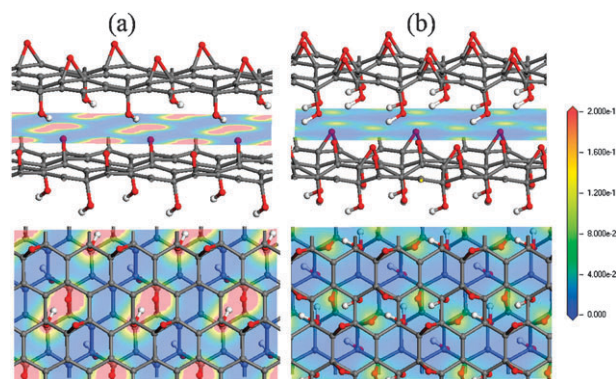
Fig. 4 Charge density at the middle of the interlayer space of less oxidized (a) and highly oxidized (b) anhydrous graphite oxide. The unit of the scale bar is electrons per Å³.

Table 3 Optimized (initial) configuration of the $C_8O_2(OH)_2$ structure

Model		A(12-45-1'2'-5'7')	S(12-45-1'2'-4'5')	A(34-28-1'2'-4'5')
Cell parameters	a/Å	5.023 (5.1)	5.050 (5.1)	5.032 (5.1)
	b/Å	5.009 (5.1)	5.016 (5.1)	5.001 (5.1)
	c/Å	11.734 (12)	12.270 (12)	11.794 (12)
	α/°	89.7 (90)	95.2 (90)	92.4 (90)
	β/°	89.2 (90)	77.8 (90)	93.3 (90)
	γ/°	119.8 (120)	120.5 (120)	119.8 (120)
OH···O (epoxide) bonding angles/°		131	119	128
		128	110	124
Relative energy/eV		0	0.11	0.07
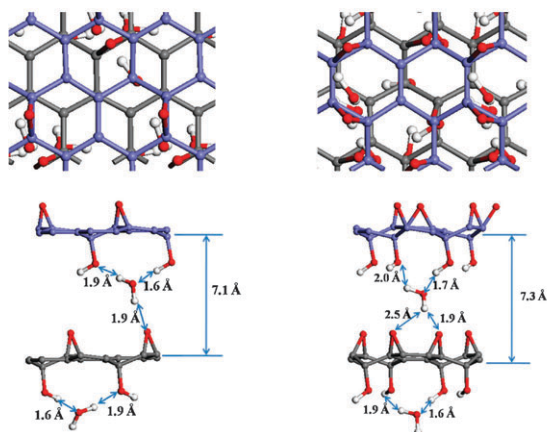
Fig. 5 Configuration along the *c* vector direction (top panel) and side view (bottom panel) of less (a) and highly (b) oxidized hydrated graphite oxide. AB stacking is not maintained in highly oxidized hydrated graphite oxide.

Table 4 Optimized (initial) configuration of the hydrated graphite oxide structure

Cell parameters	$C_8O(OH)\cdot(H_2O)$	$C_8O_2(OH)_2\cdot(H_2O)$
$a/\text{Å}$	4.964 (5)	5.013 (5)
$b/\text{Å}$	4.964 (5)	5.001 (5)
$c/\text{Å}$	13.980 (14.4)	14.631 (14.6)
$\alpha/°$	89.3 (90)	89.8 (90)
$\beta/°$	91.2 (90)	90.1 (90)
$\gamma/°$	119.6 (120)	120.0 (120)

localized more strongly near the epoxide than the hydroxyl groups, as clearly seen in the bottom panel of Fig. 4(a). This asymmetric charge distribution became more pronounced for high oxidation graphite oxide. Electron charges were mostly localized near the epoxide group. Despite the doubling of the number of epoxide and hydroxyl groups in the high oxidation graphite oxide, less electron charges are accumulated in the middle of the layer compared to low oxidation graphite oxide. We estimated the interlayer coupling energy (the energy difference between the total energy of the individual A and B single layers and that of the periodic structure). Using the local density approximation (LDA), we calculated the coupling energy of pure graphite (22 meV per carbon atom); this value is slightly smaller than the experimental value of 35 meV per carbon atom.[29] In the case of graphite oxide, it is known that the GGA can describe the hydrogen bonding better than the LDA.[26,30,31] The coupling energy of high oxidation graphite oxide is 18 meV per carbon atom, which

is smaller than 25 meV per carbon atom estimated for low oxidation graphite oxide. Thus, weak coupling resulted in a larger interlayer distance in graphite oxide with a high level of oxidation. The large interlayer distance and the asymmetric charge distribution between layers in graphite oxide are critical for its applications in supercapacitors and battery devices; furthermore, these large interlayer distances could function in hydrogen storage by providing enough room for hydrogen and enhancing the interactions between hydrogen atoms and functional groups such as epoxide groups.

3.3 Hydrated graphite oxide

In general, graphite oxide is believed to be hygroscopic, with some number of water molecules present in graphite oxide samples. The concentration of water is about 6–11% in the real samples.[10,11] In our theoretical models, one water molecule was introduced into low and high oxidation graphite oxide species, corresponding to $C_8O(OH)\cdot H_2O$ (14 wt% water) and $C_8O_2(OH)_2\cdot H_2O$ (11 wt% water), respectively, as shown in Fig. 5. In each case, the lowest energy configurations were taken from the anhydrous models (Table 4). The in-plane structural changes in the presence of a water molecule were negligible. The intercalation energy in the hydrated graphite oxide per water molecule was estimated as $\Delta E_{int} = (E_{hydrated} - E_{anhydrous} - 2E_{water})/2$. The intercalation energy values were −0.58 and −0.34 eV for the less oxidized and highly oxidized graphite oxide forms, respectively. This implies that water molecules can easily be incorporated into the interlayers and combine with the anhydrous graphite oxide *via* hydrogen bonding. This phenomenon was experimentally observed by Szabó *et al.*[10] This also explains why it is very difficult to obtain absolutely anhydrous graphite oxide in practice.

For the less oxidized hydrated graphite oxide, the AB stacking order was maintained in the presence of water, Fig. 5(a). The interlayer distance expanded from 5.1 to 7.1 Å. The hydrogen bonding was well maintained by three OH···O bonds near the water molecule, as shown in the bottom panel of Fig. 5(a). This result is consistent with the experimental data reported previously.[11] In that report, the chemical formula of the graphite oxide sample was $C_8O_{1.06}(OH)_{1.37}(H_2O)_{0.8}$—this is very close to the formula of our less oxidized model with hydration. In contrast, the AB stacking order was not maintained in highly oxidized graphite oxide with 11 wt% water. This phenomenon can be explained by the weaker interaction between layers and the formation of a greater number of multi-coordinated hydrogen bonds in highly oxidized graphite oxide. Although the number of epoxide and hydroxyl groups was doubled in highly oxidized

Table 5 Summary of coupling energies of graphite and graphite oxides

	Oxidation level	Coupling energy/meV per carbon	Origin of interaction
Graphite		35 (LDA)	van der Waals interactions
Anhydrous graphite oxide	Low oxidation	25 (GGA)	Hydrogen bond interactions
	High oxidation	18 (GGA)	
Hydrated graphite oxide	Low oxidation	112 (GGA)	Hydrogen bond interactions between the graphene oxide layers and water molecules
	High oxidation	98 (GGA)	

graphite oxide, the layer–layer interaction in highly oxidized anhydrous graphite oxide was smaller than in less oxidized anhydrous graphite oxide that is shown in Table 5. It was caused by the formation of in-plane hydrogen bonds. Fig. 3 shows that the distances of in-plane hydrogen bonds were smaller than those of interlayer hydrogen bonds. Therefore, the AB stacking related to interlayer interaction is more easily broken in highly oxidized graphite oxide. The higher number of hydroxyl and epoxide groups also created more abundant multi-coordination of hydrogen bonds and the entropic disorder is therefore provoked. This explains why the AB stacking is no longer maintained in hydrated highly oxidized graphite oxide.

4. Conclusions

We have investigated structural properties and energetics of a graphitic AB stacking order in a bulk GO model that is consistent with experimental data. The conservation of graphitic AB stacking according to different oxidation levels was evaluated. AB stacking was maintained only for anhydrous and less oxidized hydrated graphite oxide. We also considered interlayer hydrogen interactions and in-plane hydrogen inter-actions; both of them play an important role in the graphite oxide stability. The interlayer distances without and with intercalated water molecules were also estimated. The interlayer distance was determined by optimization of hydrogen bonding between functional groups in different planes in anhydrous graphite oxide, and hydrogen bonding between water molecules and functional groups in hydrous graphite oxide.

Acknowledgements

References

1 V. C. Tung, M. J. Allen, Y. Yang and R. B. Kaner, *Nat. Nanotechnol.*, 2009, **4**, 25.
2 S. Stankovich, D. A. Dikin, R. D. Piner, K. A. Kohlhass, A. Kleinhammes, Y. Jia, Y. Wu, S. B. T. Nguyen and R. S. Ruoff, *Carbon*, 2007, **45**, 1558.
3 S. Stankovich, D. A. Dikin, G. H. B. Dommett, K. M. Kohlhass, E. J. Zimney, E. A. Stach, R. D. Piner, S. B. T. Nguyen and R. S. Ruoff, *Nature*, 2006, **442**, 282.
4 H. J. Shin, K. K. Kim, S. M. Yoon, A. Benayad, H. K. Park, M. H. Jin, H. K. Jeong, J. Kim, J. Y. Choi and Y. H. Lee, *Adv. Funct. Mater.*, 2009, **19**, 1987.
5 D. A. Dikin, S. Stankovich, E. J. Zimney, R. D. Piner, G. H. B. Dommett, G. Evmenenko, S. B. T. Nguyen and R. S. Ruoff, *Nature*, 2007, **448**, 457.
6 I. J. Kim, S. Yang, M. J. Jeon, S. I. Moon, H. S. Kim, Y. P. Lee, K. H. An and Y. H. Lee, *J. Power Sources*, 2007, **173**, 621.
7 T. Nakajima and Y. Matsuo, *Carbon*, 1988, **26**, 357.
8 M. Mermoux, Y. Chabre and A. Rousseau, *Carbon*, 1991, **29**, 469.
9 A. Lerf, H. He, M. Forster and J. Klinowski, *J. Phys. Chem. B*, 1998, **102**, 4477.
10 T. Szabó, O. Berkesi, P. Forgó, K. Josepovits, Y. Sanakis, D. Petridis and L. Dékány, *Chem. Mater.*, 2006, **18**, 2740.
11 H. K. Jeong, Y. P. Lee, R. J. Lahaye, M. H. Park, K. H. An, I. J. Kim, C. W. Yang, C. Y. Park, R. S. Ruoff and Y. H. Lee, *J. Am. Chem. Soc.*, 2008, **130**, 1362.
12 H. K. Jeong, H. J. Noh, J. Y. Kim, M. H. Jin, C. Y. Park and Y. H. Lee, *Europhys. Lett.*, 2008, **82**, 67004.
13 H. He, J. Klinowski, M. Forster and A. Lerf, *Chem. Phys. Lett.*, 1998, **287**, 53.
14 W. Cai, R. D. Piner, F. J. Stadermann, S. Park, M. A. Ahaibat, Y. Ishii, D. Yang, A. Velamakanni, S. J. An, M. Stoller, J. An, D. Chen and R. S. Ruoff, *Science*, 2008, **321**, 1815.
15 H. C. Schniepp, J.-L. Li, M. J. McAllister, H. Sai, M. Herrera-Alonso, D. H. Adamson, R. K. Prud'homme, R. Car, D. A. Saville and I. A. Aksay, *J. Phys. Chem. B*, 2006, **110**, 8535.
16 J.-L. Li, K. N. Kudin, M. J. McAllister, R. K. Prud'homme, I. A. Aksay and R. Car, *Phys. Rev. Lett.*, 2006, **96**, 176101.
17 J. T. Paci, T. Belytschko and G. C. Schatz, *J. Phys. Chem. C*, 2007, **111**, 18099.
18 D. W. Boukhvalov and M. I. J. Katsnelson, *J. Am. Chem. Soc.*, 2008, **130**(32), 10697.
19 R. J. W. E. Lahaye, H. K. Jeong, C. Y. Park and Y. H. Lee, *Phys. Rev. B: Condens. Matter*, 2009, **79**, 125435.
20 Available on its web page (http://www.pwscf.org).
21 J. P. Perdew, K. Burke and M. Ernzerhof, *Phys. Rev. Lett.*, 1996, **77**, 3865.
22 J. P. Perdew, K. Burke and M. Ernzerhof, *Phys. Rev. Lett.*, 1997, **78**, 1396.
23 J. P. Perdew, K. Burke and M. Ernzerhof, *Phys. Rev. Lett.*, 1998, **80**, 891.
24 H. Monkhorst and J. D. Pack, *Phys. Rev. B: Solid State*, 1976, **13**, 5188.
25 W. Koch and M. C. Holthausen, *A Chemist's Guide to Density Functional Theory*, Wiley-VCH Verlag GmbH, Weinheim, 2001.
26 J. Ireta, J. Neugebauer and M. Scheffler, *J. Phys. Chem. A*, 2004, **108**(26), 5692.
27 A. D. Rabuck and G. E. Scuseria, *Theor. Chem. Acc.*, 2000, **104**, 439.
28 L. Rao, H. Ke, G. Fu, X. Xu and Y. Yan, *J. Chem. Theor. Comput.*, 2009, **5**(1), 86.
29 L. X. Benedict, N. G. Chopra, M. L. Cohen, A. Zettl, S. G. Loui and V. G. Crespi, *Chem. Phys. Lett.*, 1998, **286**, 490.
30 D. R. Hamann, *Phys. Rev. B: Condens. Matter*, 1997, **55**(16), R10157.
31 Y. Zhao and D. G. J. Truhlar, *J. Chem. Theor. Comput.*, 2005, **1**, 415.

This journal is © the Owner Societies 2010

Phys. Chem. Chem. Phys., 2010, **12**, 1595–1599 | 1599